Energy transfer in photosynthesis: experimental insights and quantitative models

Rienk van Grondelle*[b] and Vladimir I. Novoderezhkin[a]

Received 5th October 2005, Accepted 24th November 2005
First published as an Advance Article on the web 8th December 2005
DOI: 10.1039/b514032c

We overview experimental and theoretical studies of energy transfer in the photosynthetic light-harvesting complexes LH1, LH2, and LHCII performed during the past decade since the discovery of high-resolution structure of these complexes. Experimental findings obtained with various spectroscopic techniques makes possible a modelling of the excitation dynamics at a quantitative level. The modified Redfield theory allows a precise assignment of the energy transfer pathways together with a direct visualization of the whole excitation dynamics where various regimes from a coherent motion of delocalized exciton to a hopping of localized excitations are superimposed. In a single complex it is possible to observe the switching between these regimes driven by slow conformational motion (as we demonstrate for LH2). Excitation dynamics under quenched conditions in higher-plant complexes is discussed.

1. Introduction

Photosynthesis is at the basis of life on this planet. Solar photons are absorbed by a complex system of membrane-associated pigment-proteins (light-harvesting antenna) and the electronic excited state is efficiently transferred to a reaction center (RC), where it is converted into a transmembrane electrochemical potential difference.[1,2] Antenna complexes consist of ordered arrays of light-harvesting pigments (*i.e.* chlorophylls (Chl) or bacteriochlorophylls (BChl) as main pigments together with other cofactors) bound to proteins. Following the discovery in 1975 of the structure of the FMO complex of green bacteria,[3] high-resolution studies performed between 1995–2005 revealed structures for LH2[4–6] and LH1[7–9] complexes of purple bacteria, for the major light-harvesting complex LHCII of higher plants,[10–12] and core complexes of photosystem I[13] and photosystem II.[14–16] The bacterial light-harvesting complex LH2 consists of highly symmetric rings of 9 (or 8) pigment-protein subunits, each containing two transmembrane polypeptide helixes and three BChls, forming tightly packed circular aggregates of 18 (16) BChls with the second ring of 9 (8) weakly interacting BChls.[4–6] The LH1 antenna has 16 or 15 subunits with two BChls each, forming circular structures with 32 BChls[7,8] or an open circle with 30 BChls[9] surrounding the RC. Complexes from higher plants have a bigger number of pigments, from 42 Chls in LHCII[11] to 96 Chls in the PSI-core,[13] arranged less regularly in two parallel layers close to the stromal or lumenal surface of the membrane. The average distance between nearest-neighbour pigments can be as short as 12 Å in FMO, 9.7–12.8 Å within each layer in LHCII, and 8.9–9.2 Å in the inner ring of LH2 antenna, thus giving rise to strong pigment–pigment interactions. As a result, the whole antenna is generally characterized by a complicated manifold of the excited states, including collective electronic excitations (excitons) with a high degree of delocalization in combination with more localized excitations due to the presence of weakly coupled pigments.

Modulation of the electronic transition energies by slow conformational motion of the protein matrix produces disorder of the site energies within a single complex (thus resulting in more localized exciton wavefunctions) as well as inhomogeneous broadening of the electronic transitions due to ensemble averaging.

Coupling of excitations to a fast nuclear motion (intra- and interpigment vibrations, phonons) results in: (i) homogeneous broadening of the electronic transition spectra, (ii) their red shift due to reorganization effects (associated with changes in equilibrium position of the nuclear modes after electronic excitation), (iii) a further decrease of the delocalization size due to polaron effects, and (iv) the transfer of electronic excitation within the excited state manifold, including fast (fs) relaxation between exciton states within strongly-coupled clusters and slower (ps) energy migration between clusters or monomeric sites.

In native antenna complexes excitations are coupled to a continuum of low-frequency phonons and to several dozens vibrational modes with frequencies up to 1700 cm^{-1} (as revealed by hole-burning,[17] fluorescence line-narrowing,[18–21] inelastic neutron scattering[22] measurements and molecular dynamics simulations[23]) allowing energy transfer between excited states belonging to the same or to different spectral bands. This energy transfer is the basic mechanism of photosynthetic light-harvesting producing ultrafast cascading from higher- to lower-energy states and an effective energy migration in the antenna and the delivery of excitation energy to the RC. Since the biochemical isolation of antenna complexes and the discovery of their structure the fast energy transfer events have been studied using a variety of advanced laser spectroscopic methods, including time-resolved (sub-100 fs) nonlinear

[a] *A. N. Belozersky Institute of Physico-Chemical Biology, Moscow State University, Leninskie Gory, 119992 Moscow, Russia*
[b] *Department of Biophysics, Faculty of Sciences, Vrije Universiteit, De Boelelaan 1081, 1081 HV Amsterdam, The Netherlands. E-mail: rienk@few.vu.nl; Fax: +31-20 5987999; Tel: +31-20 5987930*

techniques together with theoretical modeling (for a review see ref. 2, 24–28).

In the simplest version of theory the dynamics is described in a pure exciton basis, where exciton relaxation is accounted for by including exciton–phonon coupling as an off-diagonal perturbation (Redfield theory[29]). Such an approach was used to model the dynamics within the B850 band of LH2,[30–32] intra- and interband B800–B850 transfers in the whole LH2 antenna,[33,34] intra- and interband dynamics in the Chl *b*-Chl *a* LHCII complex,[35] equilibration dynamics in FMO,[36,37] equilibration dynamics in the PSI core,[38] and energy/electron transfer in the PSII-RC.[39–41]

In the modified version of the Redfield theory[42,43] the diagonal (in the exciton basis) part of the electron–phonon coupling is taken into account non-perturbatively, thus giving more realistic line shapes and relaxation rates due to the inclusion of multiphonon processes.[44] Such a theory allowed a better quantitative treatment of spectra and dynamics in PSI,[45] LHCII,[46,47] and the PSII-RC.[48,49] Recently the theory was used to model the 2D-photon echo spectra in FMO.[50]

Besides the relatively weak coupling to the bath, inducing relaxation phenomena, the excitations in pigment–protein complexes can be strongly coupled to a few low-frequency vibrational modes. In this case the nonlinear spectral responses will exhibit oscillations due to long-lived vibrational coherences, which have frequently been observed in bacterial RCs,[51–58] in bacterial LH1/LH2 antennas,[59–66] chlorosomes,[67,68] and in LHCII.[69] Modeling of the coupled electronic and vibrational dynamics in this case requires theory with nuclear degrees of freedom included explicitly as system coordinates. The relaxation in such a system can be described using the Redfield theory in the basis of electron-vibrational eigenstates. This approach allowed description of the electron transfer coupled to coherent nuclear motion in the bacterial RC,[70–73] exciton-vibrational relaxation in Chl *a*-*b* heterodimers from LHCII,[74,75] long-lived vibrational coherences in LH1,[76,77] and coupled exciton-vibrational relaxation in LH1.[26,78]

Coupling of electronic excitation to slow conformational changes of the antenna produces different disorder patterns viewed in conventional bulk spectroscopies as inhomogeneous broadening. An extent of inhomogenous broadening and the influence of the disorder on the exciton states has been studied by hole burning spectroscopy.[79–81] The dynamics of conformational changes can be monitored directly using single-molecule techniques.[82,83] Spectral fluctuations on the microsecond to second timescale observed in a single-molecule experiment[84–95] are associated with the evolution of the antenna complex through a number of conformational substates. Single molecule studies allowed for the first time an acquisition of line shapes and polarizations of exciton states of a single LH1/LH2 complex.[87,96,97] Secondly, statistics of different types of disorder became available, for example, the ratio of the inter- and intra-complex energetic disorder, which are not distinguishable with conventional methods.[90] Finally, the spectral signatures of slow conformational changes gave information about the static disorder patterns[94,95] (and specific types of the excitation dynamics (V. Novoderezhkin *et al.*, submitted)) produced by different conformational sub-states.

In this paper, we overview experimental findings for the LH1, LH2, and LHCII complexes obtained with various techniques highlighting coupled exciton-vibrational dynamics in LH1, interplay of intra- and interband transfers in LH2 and LHCII complexes, and slow conformational dynamics of single LH2 complex. Knowledge of the structure,[4,5,8,11,12] the effective dipole moments of Chls and BChls[98] and the spectral density of electron–phonon coupling[18,23] for these complexes allows modelling of the spectra and excitation dynamics at a quantitative level. We demonstrate that a simultaneous fit of the linear and nonlinear spectral responses using Redfield theory yields a precise determination of the site energies, the only unknown parameters necessary to develop a complete scheme of photosynthetic energy transfer. Moreover, once we obtain these site energies a direct comparison with quantum–chemical calculations becomes possible.

2. Structure and exciton spectra of LH1/LH2 bacterial antenna

The B800-B850 LH2 antenna consists of two rings of BChl *a* molecules bound to a protein scaffold: the outer ring has an absorption maximum around 800 nm while the inner ring absorbs around 850 nm. Fig. 1 shows the structure of LH2 of *Rhodospirillum (Rs.) molischianum*[5] (containing 8 and 16 BChls in the outer and inner rings, respectively) together with the measured[99] and modeled[34] absorption spectra. The model gives eight exciton components in the 815–900 nm region corresponding to the lowest Davydov component of the inner ring (B850 states). The lowest $k = 0$ level, forbidden in the case of a homogeneous ring, becomes dipole allowed (even superradiant[100]) after including the disorder of the site energies. The next two most intense levels correspond to the $k = \pm 1$ states, whereas higher states are only weakly allowed due to disorder-induced mixing with the $k = \pm 1$ ones. The 770–815 nm region consists of eight exciton states of the outer ring (B800 states) mixed with the eight states from the upper Davydov component of the inner ring (B850* states).

The energy transfer dynamics includes migration of localized excitations around the BChl 800 outer ring, superimposed on the transfer to the exciton states of the BChl 850 inner ring with subsequent equilibration in the B850 exciton manifold and the motion of the quasi-steady-state wavepacket (delocalized over 4–6 BChl's 850) around the inner ring (see refs. 25–27 for review). The possible interplay of intraband B800 → B800 and interband B800 → B850 energy transfer has been the subject of intense studies by hole burning,[101–106] pump–probe,[63,99,107–115] and three-pulse photon echo techniques[116,117] together with theoretical modeling[34] (see Section 5). The steady-state spectrum of the B850 band was studied by polarized light spectroscopy,[118] hole-burning,[119–121] superradiance,[100] CD,[122–124] Stark spectroscopy[125] and single-molecule techniques.[84–90,94,95] The dynamics within this band was studied by fs fluorescence up-conversion,[126] relative measurements of the induced absorption changes,[127] polarized pump–probe,[128–131] and photon-echo.[63,64] Modeling has included *ab initio* calculation of the exciton Hamiltonian,[23,28,132–135] quantitative fitting of linear[23,34,124,132] and nonlinear bulk responses,[30,32,34,127] as well as lineshapes[94–97] and spectral

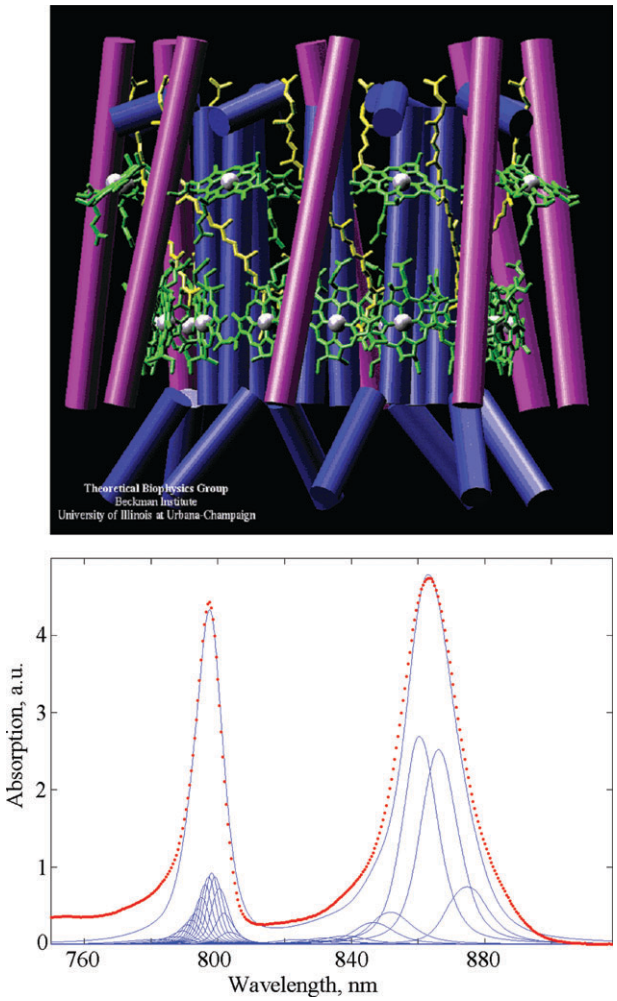

Fig. 1 Top frame: Structure of LH2 antenna of *Rs. molischianum*.[5] Bottom frame: The absorption spectrum of the LH2 antenna of *Rs. molischianum* measured at 77 K[99] (points) and calculated using the standard Redfield theory[34] (solid lines). The calculated absorption is shown together with contributions of the individual exciton components.

fluctuations[94,95] in a single complex. The precise character of the excitation within the circular aggregates of the B850-LH2 and LH1 antennae, such as the degree of delocalization, multiple coherence sizes, dynamic localization, *etc*. has been the subject of intense debate[62,100,119,129,132,136–142] and was critically reviewed and summarized in refs. 127, 143 and 144.

The LH1 antenna has a structure similar to that of the B850 ring of LH2.[7–9] The larger size (30–32 BChls instead of 16–18 in LH2) results in less spacing between zero-order exciton levels, which in turn produces stronger disorder-induced mixing of the exciton states (Fig. 2A). In particular, the lowest $k = 0$ state becomes more superradiant,[100] and the higher $k = \pm 2$ states (almost forbidden in LH2) now give a significant contribution to the absorption profile. This feature is responsible for the larger amplitude of the dynamic Stokes shift observed in LH1 as compared with LH2.[66,78] Another specific property of LH1 is the stronger coupling to low-frequency vibrations, manifested as more pronounced oscillatory features in nonlinear responses due to vibrational coherences.[66,76,77]

3. Equilibration dynamics in LH1 and B850-LH2

3.1. Exciton relaxation dynamics

The direct observation of the excitation dynamics in the tightly packed ring-like aggregates of LH1 and B850-LH2 antenna (including relaxation of the exciton states and migration of the quasi-steady-state exciton wavepacket) is possible by transient absorption (TA) studies *via* the ps/fs pump–probe technique. Such measurements have revealed the initial ultrafast (sub-100 fs) relaxation in LH1/LH2 complexes followed by slower (ps) dynamics.[66,113,128–131,145–151]

Fast relaxation in such a system gives rise to specific TA dynamics that is typical for assemblies of excitonically coupled antenna pigments, but is absent in isolated dimeric subunits and monomers. Thus, Visser *et al.*[146] found a pronounced TA dynamics for LH1 of *Rhodospirillium rubrum* with an 8–12 nm red shift reflecting fast exciton equilibration, whereas no red-shift dynamics were found in the lowest-state absorption band of the B820 dimeric subunit as well as for monomeric BChl.

A short-pulse (35–50 fs) pump–probe study of LH1 and LH2 of *Rhodobacter sphaeroides*[128–131] showed relaxation components in the 10–100 fs range (short-lived <20 fs components appear when tuning the wavelength to the blue[130]). Selective excitation with longer pulses at the blue side of the LH2 absorption resulted in a dynamic red shift of the TA spectrum by 3–5 nm with a time constant of 80–110 fs.[129,131] This shift (attributed to relaxation from higher to lower exciton levels) was almost absent upon red excitation.

Upon blue-side excitation of the LH1 of *Rhodopseudomonas (Rps.) viridis*[66] a dynamic red shift was observed with a time constant of 130–150 fs accompanied by an anisotropy decay with a similar time constant of about 150 fs. The amplitude of this red shift (15–20 nm) is several times larger than in LH2 and is similar to that obtained for other LH1 antennae in earlier experiments.[145,146] Upon tuning the excitation wavelength to the middle of the band the dynamic red shift becomes less pronounced. In addition to this ultrafast red shift more long-lived oscillatory features were observed (see next section).

This coupled exciton-vibrational dynamics was explained quantitatively using the Redfield relaxation theory.[78] At delays shorter than 400 fs, the TA dynamics are determined mostly by a large dynamic red shift due to fast exciton relaxation (Fig. 2B). The theory predicts shorter lifetimes for higher levels due to predominant downhill relaxation (Fig. 2E). Therefore, tuning the excitation wavelength to the blue results in a faster relaxation with a concomitant increased amplitude of the red shift. The data is reproduced by the disordered exciton model assuming an uncorrelated disorder of the site energies[78] (Fig. 2C and D). In the disordered model the red-shift dynamics upon blue-side excitation is determined by relaxation from strongly allowed higher $k = \pm 2$ levels (Fig. 2A). Upon middle-band excitation, corresponding to excitation of the $k = \pm 1$ levels the red shift is much less pronounced (compare C and D frames of Fig. 2). It is of some interest to discuss models with correlated disorder for instance due to elliptical deformations,

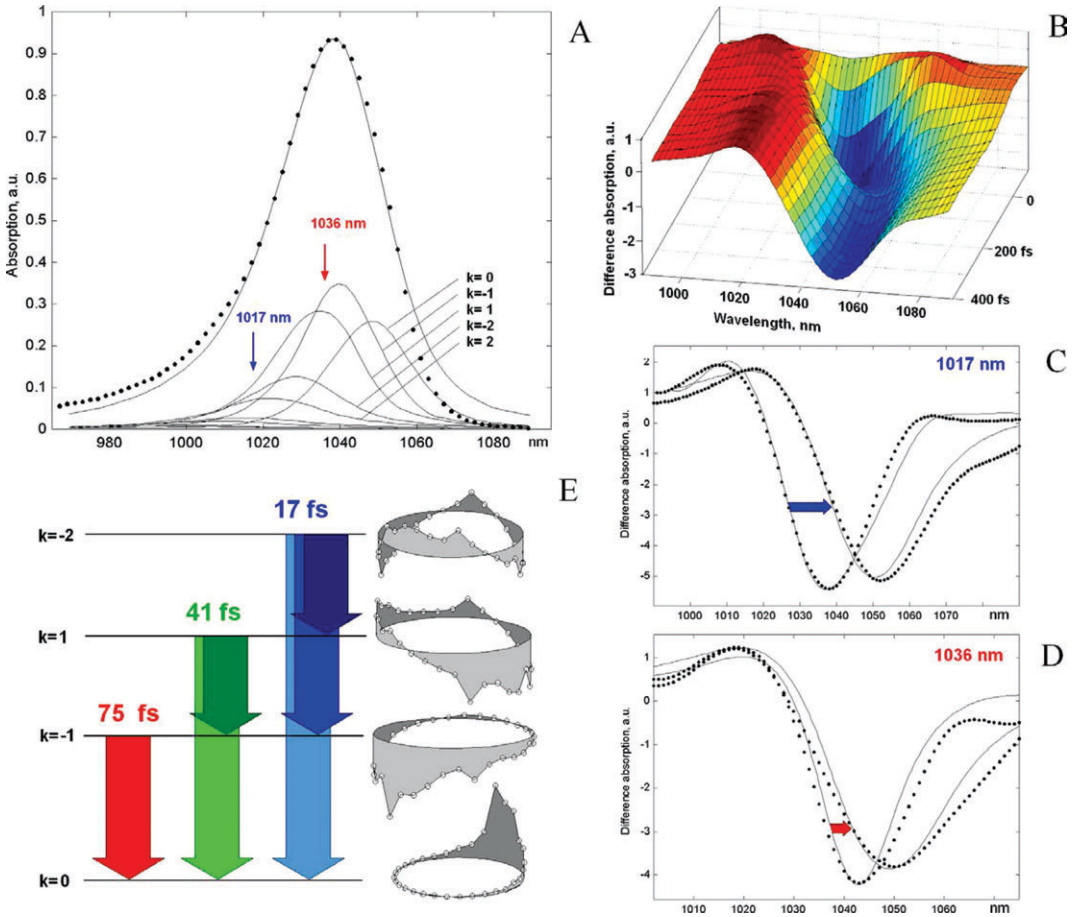

Fig. 2 A: Measured[66] (points) and calculated[78] absorption (solid lines) of the LH1 of *Rps. viridis* at 77 K. The calculated absorption is shown together with contributions of the individual exciton components. B: Dynamics of the TA spectrum measured upon 1017 nm excitation.[66] C, D: Red shift of the pump–probe profiles between 0 and 400 fs upon 1017 and 1036 nm excitation. Experimental data[66] is shown by points, calculated spectra,[78] by solid lines. E: Exciton wavefunctions c_n^k (participation of the n-th pigment of the ring in the k-th exciton state) for $k = 0$, -1, 1, and -2 calculated for one realization of the disorder. Arrows show downhill relaxation between these levels, giving a predominant contribution to their lifetimes at 77 K (averaged over disorder lifetimes are 75, 41, and 17 fs for $k = -1$, 1, and -2, respectively).

correlated shift of the site energies, *etc*. In that case the absorption spectrum is determined mostly by the $k = \pm 1$ states, whereas the $k = \pm 2$ states remain forbidden.[94–97] As a consequence the red-shifting of the TA upon blue excitation is almost the same as for middle-band excitation, in contradiction with the experiment.

3.2. Interplay of excitonic and vibrational coherences

Excitation dynamics in ring-like antenna complexes LH1 and B850-LH2 studied in the sub-ps to ps time range using femtosecond pump–probe,[59–61,65–68] fluorescence upconversion,[62] transient grating,[63,64] and photon-echo spectroscopies[64,69] revealed pronounced oscillatory features due to vibrational coherences. These coherences were found to be more intense and more long-lived in LH1. Thus, experimental studies of the TA dynamics for the LH1 antenna of *Rps. viridis*[66] revealed coupling to two vibrational modes with frequencies of 48–65 and 103–108 cm^{-1}, which produce oscillations in the TA signals persistent during 1–1.5 ps with a surprisingly large damping time constant (600–800 fs). This time significantly exceeds the time of exciton relaxation or hopping as determined by the ultrafast redshift of the difference absorption and by anisotropy decay.

The oscillatory features due to vibrational coherences have smaller amplitude than the red-shift TA dynamics at short delays (<200 fs), but at larger delays (after exciton relaxation) the oscillations are clearly distinguishable. Modeling of the wavelength-dependent oscillatory pattern was performed using the Redfield theory in the basis of exciton-vibrational eigenstates.[77] The impulsive excitation of electronic levels coupled to specific nuclear modes creates a wavepacket in nuclear space (both in the ground state and in the one-exciton manifold). Coherent motion of the ground state wavepacket yields oscillations in the photobleaching (PB), whereas the excited state wavepacket produces similar oscillations (but with different phase) in the one-exciton stimulated emission (SE) and the one-to-two exciton absorption (ESA). Superposition of these three components results in a complicated wavelength-dependent pattern of oscillations in the total TA signal, that can be reproduced quantitatively by the model (Fig. 3). The simultaneous fit of the TA traces upon different

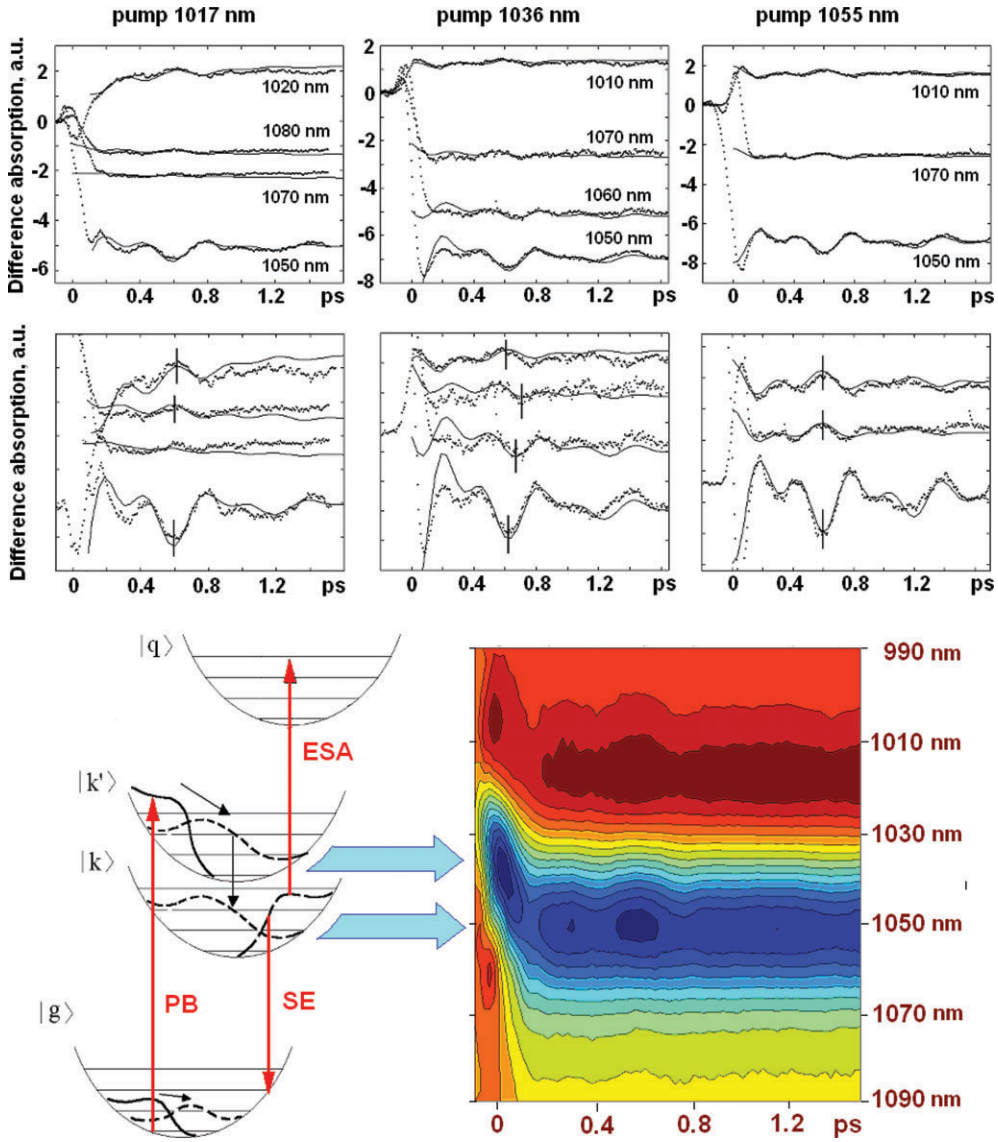

Fig. 3 Top: Measured[66] and modeled[77] TA traces upon blue (1017 nm), middle (1036 nm) and red-side (1055 nm) excitation of the LH1 antenna of *Rps. viridis* at 77 K. Detection wavelengths are from 1010 to 1080 nm as indicated. The lower frames show the same data, but the timetraces are shifted in the vertical direction for easy comparison. Bottom: The ground (g), one-exciton (k, and k') and two-exciton (q) potential energy curves together with the evolution of the ground- and excited-state vibrational wavepackets during the first oscillatory half-period (this oscillatory motion modulates the ESA, PB, and SE amplitudes). On the right the oscillatory features of the experimental TA spectrum are shown (colors in the contour diagram are the same as in the 3D plot in Fig. 2B). The fast red shift of the TA during 0–0.1 ps reflects relaxation of the wavepacket from k to the lower k' state. Oscillatory features in the blue (1030–1000 nm) and red side (1050–1090 nm) are determined by contributions from ESA and PB/SE, respectively.

excitation/detection wavelengths yields precise estimates of the frequencies, coupling parameters, damping constants of the nuclear modes (for details see ref. 77).

It is important to note that the relaxation of the initially created exciton wavepacket within 150 fs (shown in Fig. 2 and 3) does not shorten the long-lived (within 1–1.5 ps) coherent oscillations. However, further migration of the wavepacket along the circular antenna will induce an additional decay of the vibrational coherences. The time constant of this decay estimated from the fit of oscillatory patterns as τ_{hop} = 0.9–1.5 ps[77] was taken to be the effective time of migration over a distance comparable with the delocalization length. The latter is equal to 8 BChl molecules at 77 K[78,152]. Notice that at room temperature the delocalization length in LH1/LH2 is 4–6 BChls.[26,30,127,152] The hopping time of the wavepacket in this case must be shorter. Thus, the modeling of the room-temperature single-molecule LH2 data (see next section) gave τ_{hop} = 350 fs.

4. Variety of excitation dynamics in B850-LH2 revealed by single molecule spectra

Studies of excitation dynamics with conventional bulk spectroscopies, although sensitive to details of the dynamics on the fs timescale, are restricted to averaging over disorder (*i.e.* over a large number of complexes in different conformational states).

Contemporary single molecule techniques have no fs/ps resolution, but allow a direct visualization of the conformational changes of individual complexes (through their spectral signatures) on a ms/s timescale.

Based on low- and room-temperature single molecule experiments it has been proposed that the LH2 ring can deviate from the ideal circular structure.[84–90] The anomalously large splitting of the two major orthogonal excitonic transitions of the B850 band observed in polarized FL excitation spectra was accounted for by introducing correlated shifts of the site energies (or interaction energies) due to an elliptical deformation and reducing the amount of uncorrelated disorder.[87,88,96,97]

On the other hand, the changes in the FL profile related to the abrupt movements of the FL peak[94,95] strongly suggest a large value of uncorrelated disorder in LH2. Modeling based on the modified Redfield theory (V. Novoderezhkin *et al.*, submitted) showed that the experimentally observed spectral fluctuations reflect the evolution of the complex through a number of conformational sub-states with specific disorder patterns producing different types of emission profile and corresponding to different regimes of the excitation dynamics.

Fig. 4 shows averages of experimentally observed and calculated FL profiles with blue-shifted (859–861 nm), intermediate (869–871 nm), and red-shifted (889–891 nm) peak position. Red-shifted single molecule profiles on average are significantly broadened and have a specific shape with a broader short-wavelength wing. Spectra with intermediate and blue-shifted peak position feature regular FL asymmetry, *i.e.* a broader long-wavelength tail. Notice that blue-shifted spectra are also broader than those with intermediate peak position. The modeling revealed that the spectra for these three classes of realizations correspond with three different types of exciton structure characterized by different relative

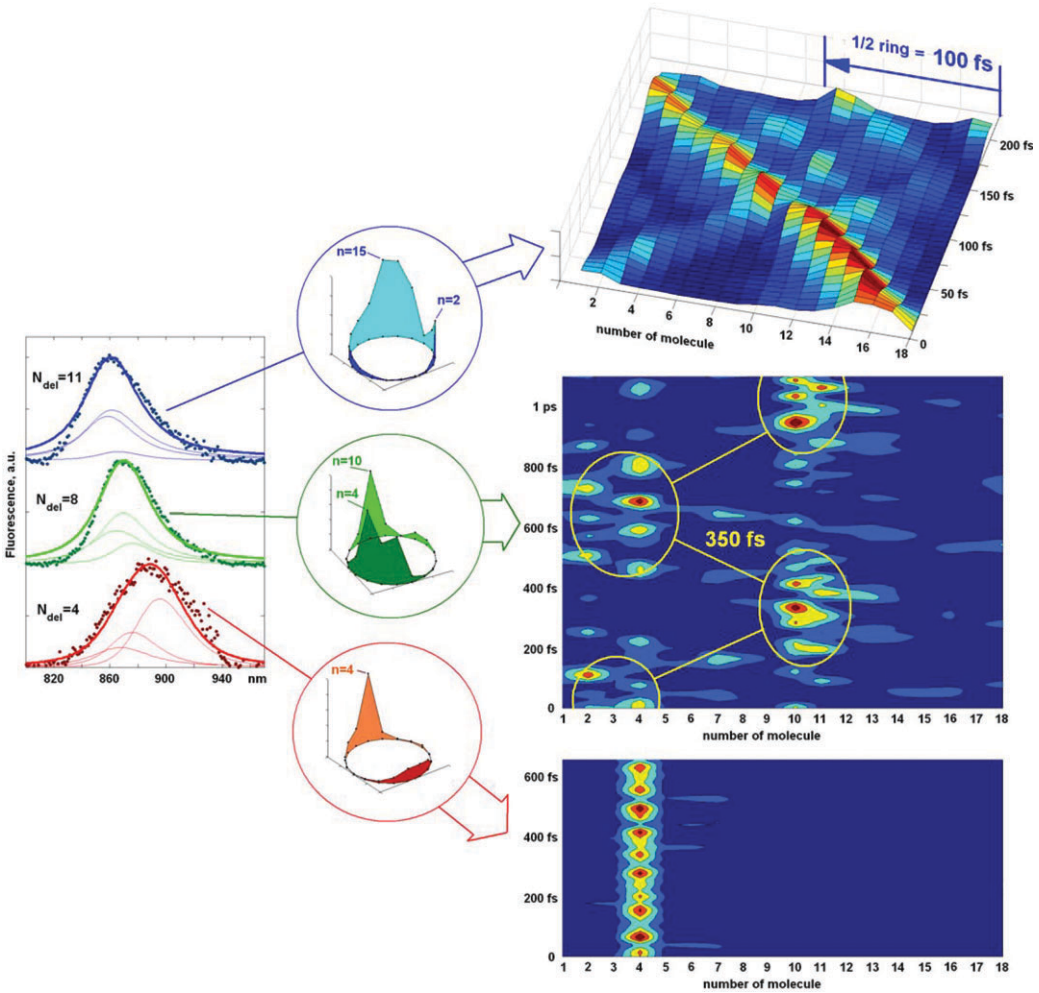

Fig. 4 Left frames: Measured (points) and calculated (solid) fluorescence profiles of single LH2 complex from *Rhodopseudomonas (Rps.) acidophila* at room temperature corresponding to realizations with the peak positions in the range 859–861 nm (top), 869–871 nm (middle), and 889–891 nm (bottom). Calculated FL profiles are shown together with contributions of the three lowest exciton states (thin solid). N_{del} is the delocalisation of the individual exciton wavefunctions defined as the inverse thermally averaged participation ratio. Inserts in the middle: The shape of the room-temperature wavepacket for a characteristic realization taken from each of the three groups. Right frames: Coherent dynamics of the density matrix, *i.e.* calculated without relaxation of populations and coherences. The initial population corresponds to thermal equilibrium at room temperature, initial coherences have arbitrary fixed phases. Diagonal elements of the density matrix in the site representation $\rho(n,n)$ are shown as a function of time for the same realizations as in the middle.

positions, line shapes, and delocalization of the lowest exciton components $k = 0$, $k = -1$, and $k = 1$.

The exciton states in the blue-shifted realizations are not significantly destroyed by the disorder. As a result the exciton structure in this case is also not too different from that of the homogeneous ring, *i.e.* most of the dipole strength is concentrated in two degenerate levels ($k = \pm 1$), whereas the lowest state ($k = 0$) is almost forbidden due to the symmetry of the ring. The room-temperature emission originates mostly from the degenerated $k = \pm 1$ pair giving rise to a blue-shifted FL.

FL profiles with intermediate peak position result from realizations of stronger static disorder. This situation corresponds to an increase in splitting between the exciton levels and a more localized character of exciton states. The red-shifted and more localized $k = 0$ state also becomes more radiant borrowing some of the dipole strength from higher levels so its contribution to the FL profile becomes more significant.

For the red-shifted FL profiles the exciton structure is very strongly affected by the disorder, which causes a large splitting between the energy levels, in particular, the splitting between the $k = \pm 1$ and the lowest $k = 0$ state is increased significantly (as compared with the blue-shifted and intermediate spectral profiles). Due to this large splitting between excitonic energy levels most of the FL originates from the lowest state, which is now strongly allowed and red-shifted. Its localized character gives rise to an increase of effective phonon coupling. Such increased coupling results in a broadening of the FL profile together with an additional red shift.

It is important to note that the shape of the FL profile with intermediate and red-shifted peak position is largely determined by the shift and broadening of the $k = 0$ level, a feature that is the key property of the disordered ring and which is absent in the case of correlated disorder (where the $k = 0$ state is almost forbidden). As a result the model with correlated disorder yields only a limited shift of the spectrum without significant changes of its shape.

The increased splitting between the levels accompanied by enhanced phonon coupling is the origin of the increasingly larger broadening of the FL spectra in red-shifted realizations. Another line broadening factor that determines the width of the blue-shifted FL spectra is exciton relaxation. Typically due to predominant downhill relaxation the inverse lifetime increases for higher levels. Thus the more pronounced relaxation broadening of the $k = \pm 1$ levels causes the larger width of the blue-shifted FL spectra (determined mostly by the $k = \pm 1$ emission).

The dynamics of the exciton wavepacket given by the time evolution of the density matrix in the site representation shows three different regimes corresponding to the three types of realizations (Fig. 4). Dynamics calculated for the blue realization shows a wavelike motion of the wavepacket delocalized over 4–5 molecules around the ring. (Notice that the delocalization length of the wavepacket is less than $N_{del} = 11$ for individual wavefunctions). The initially created wavepacket has its maximum at $n = 15$–16 (see Fig. 4) and in addition a smaller maximum at $n = 2$. The passage of the main maximum over half the ring occurs in 100 fs. At this point the main maximum collides with the second maximum moving in the opposite direction.

For the second realization the excitation is delocalized over the sites $n = 2$–4 or $n = 10$–13. The dynamics are strongly reminiscent of hopping from one group of pigments to another with a time constant of about 350 fs. The wavelike motion is almost absent, but it is possible to recognize some wavelike flow of excitation density from one group to another through the intermediate site $n = 7$. Due to strong disorder the wavelike motion is destroyed by scattering on impurities, producing many secondary waves moving in both directions. This results in a complicated non-uniform standing-wave pattern with oscillating populations at some sites (whereas other sites are almost not populated). Of course in an ensemble experiment a mixture of the wavelike motion and hopping-type dynamics with the time constants of 100 and 350 fs will determine the dynamics as reflected by the fluorescence anisotropy decay. This estimation is in agreement with the observed bi-exponential fluorescence anisotropy decay with 100 and 400 fs components in fluorescence up-conversion experiments for LH1[62] and the B850 ring of LH2.[126]

In the third realization of the static disorder the excitation stays on the $n = 4$ site without any hopping to one of the other sites. But there is still some oscillatory modulation of the $n = 4$ population due to small coherences between the $n = 4$ and neighboring sites.

We conclude that the realizations of static disorder observed in single molecule experiments corresponds to physically different limits of the excitation dynamics, *i.e.* coherent wavelike motion of a delocalized exciton (with a 100 fs pass over half the ring), hopping-type motion of the wavepacket (with 350 fs jumps between separated groups of 3–4 molecules), and self-trapping of the excitation that does not move from its localization site.

5. Competition of intraband B800-800 and interband B800-850 energy transfer in LH2

Since the discovery of the crystal structure of the peripheral B800-B850 LH2 antenna of purple bacteria *Rps. acidophila*[4] and *Rs. molischianum*[5] considerable efforts have been made to understand the physical origins and pathways of the excitation energy transfer within these B800-B850 complexes. One of the most puzzling and intriguing questions is the interplay of intraband B800 → B800 and interband B800 → B850 energy transfers,[99,101–117] where migration of localized B800 excitations is superimposed with their resonant and off-resonant coupling to the upper and lower Davydov components of the B850 exciton manifold.

Typically pump–probe kinetics measured in the B800 band show a biexponential decay of the isotropic TA.[99,107–115] A slow component of 1.2–1.9 ps is taken to reflect the B800 → B850 transfer, whereas a fast phase of 0.3–0.8 ps is assigned to the B800 → B800 hopping. The anisotropy decays with approximately the same (about 0.3–0.5 ps) time, thus lending support to the assignment of the fast component to the intraband B800 → B800 transfer.

The modelling of energy transfer within B800-B850 complexes was performed using the generalized Förster theory[153–156]

and Redfield theory.[33,34] The generalized Förster theory considers arbitrary delocalization within donor and acceptor states, but the wavefunction overlap between them is treated perturbatively, thus allowing population transfers between the two (generally strongly coupled) clusters in the weak coupling limit. In the Redfield theory all exciton couplings are taken into account explicitly, thus allowing a description of all types of transfers including exciton relaxation within strongly coupled clusters and dynamics of the coherences between one-exciton states. The latter is important for a correct interpretation of the assignment of the B800 → B800 dynamics[34] (see Section 5.2).

5.1. Excitation-wavelength dependent decay of B800 band

An example of one-color polarized TA kinetics measured for *Rs. molischianum* at 77 K[99] and modeled with the Redfield theory[34] is shown in Fig. 5. The isotropic kinetics slow down when tuning the excitation to the red side of the 800 nm band, but they become faster again in the red-most edge of the band. The anisotropy kinetics show a fast decay (from 0.42 to 0.2 with about 0.5 ps time constant) which is followed by a slower ps decay (from 0.2 to 0.1 between 1 and 8 ps delay). All these features are satisfactorily reproduced by a model taking into account all the excitonic interactions (including BChl 800–800 and BChl 850–800 couplings), site inhomogeneity (which mix the forbidden B850* states near 800 nm with the B800 band), and the full Redfield relaxation tensor (including relaxation of one-exciton populations and coherences between one-exciton states as well as non-secular terms, like coherence transfer). From this model a detailed picture of the energy transfer pathways in LH2 complex has emerged as shown in Fig. 6 (for more details—see ref. 34).

5.2. Dynamics of the B800-800 and B800-850 transfers

Blue-side excitation of the B800 band creates a coherence between pairs of the B800 states, which decays with a time constant of 0.3–0.5 ps. This is followed by a slow migration of the localized exciton around the BChl 800 ring with the time constant of 1–3 ps (depending on the relative energies of neighbouring BChls). In the energy level diagram such a migration corresponds to a population of the lowest state of the B800 excited state manifold (as shown in Fig. 6, right frame). The fast decay of one-exciton coherences is mirrored by the sub-ps anisotropy decay from 0.4 to 0.2, whereas slow migration produces further ps depolarisation from 0.2 to 0.1. Note, that a calculation without including coherences (taking into account the population dynamics only) gives an initial anisotropy of about 0.2 which decays to 0.1 with a few ps time constant, thus reproducing the experimental anisotropy dynamics for delays larger than 1 ps (Fig. 5). Therefore, we conclude that the fast anisotropy decay is not connected with any energy migration around the ring (as was thought during the past 10 years[107–115]). Actually, the real B800 → B800 population transfer is relatively slow, even slower than the B800 → B850 transfers (that has a time constant of about 1 ps—see Fig. 6).

Besides direct B800 → B850 transfer there is an additional pathway of energy transfer from the outer to inner ring, *i.e.* transfer through the B850* band. The effectiveness of this channel is determined by fast (600–800 fs) B800 → B850* transfer, followed by even faster (60–200 fs) B850* → B850* and B850* → B850 relaxation. The relative contribution of the B800 → B850* → B850 pathway is equal (or at least comparable) to the contribution of the direct B800 → B850 transfer. Notice that fast back B850* → B800 transfer can in principle contribute to the fast anisotropy decay at 800 nm, but such a 'detour' pathway B800 → B850* → B800 (suggested in refs. 27, 33 and 104) is not significant due to fast B850* → B850* and B850* → B850 relaxation.

Excitation dynamics in the site representation is shown in Fig. 6. At the very first moment, in the leading edge of the pulse, we observe an almost uniform, coherent excitation of the whole BChl 800 ring (see the panel for −0.1 ps which displays a more or less uniform excitation of populations $\rho(n,n)$ and coherences $\rho(n,m)$ for n,m = 1–8). There is also

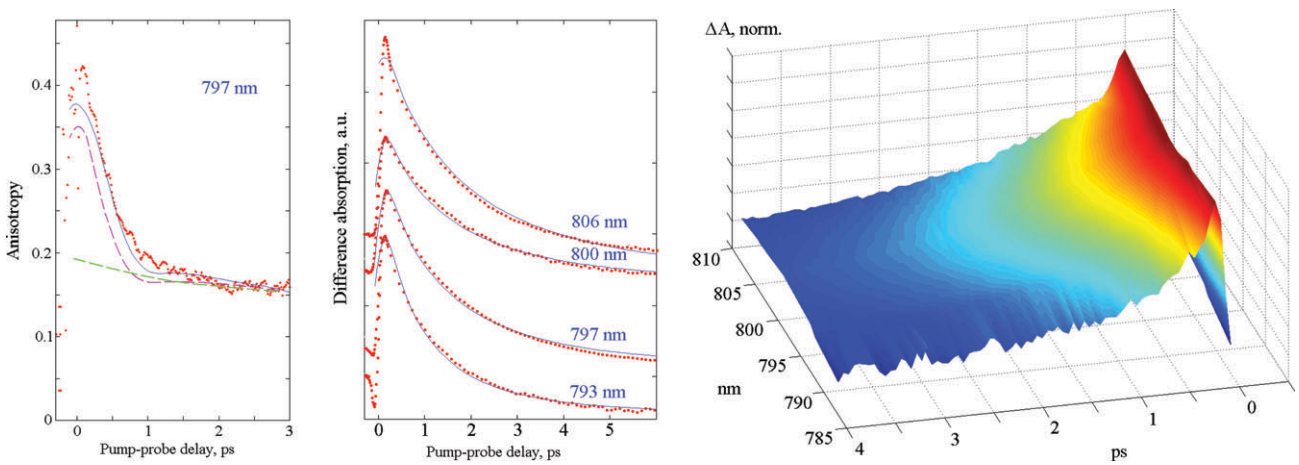

Fig. 5 Right. One-color isotropic (magic angle) pump–probe kinetics measured for the LH2 antenna of *Rs. molischianum* at 77 K upon excitation in the 800 nm region.[99] The difference absorption values are normalised to the maximal bleaching amplitude (reached near zero delay) and inverted. Middle. Fitting of the magic angle kinetics for different excitation wavelengths: experiment (points) and calculation (solid lines). Left. Fitting of the anisotropy kinetics at 797 nm: experiment (points) and calculation (solid lines). The anisotropy kinetics at 797 nm was calculated using the non-secular Redfield theory (blue), in the secular approximation (magenta) and in the non-coherent limit (green).

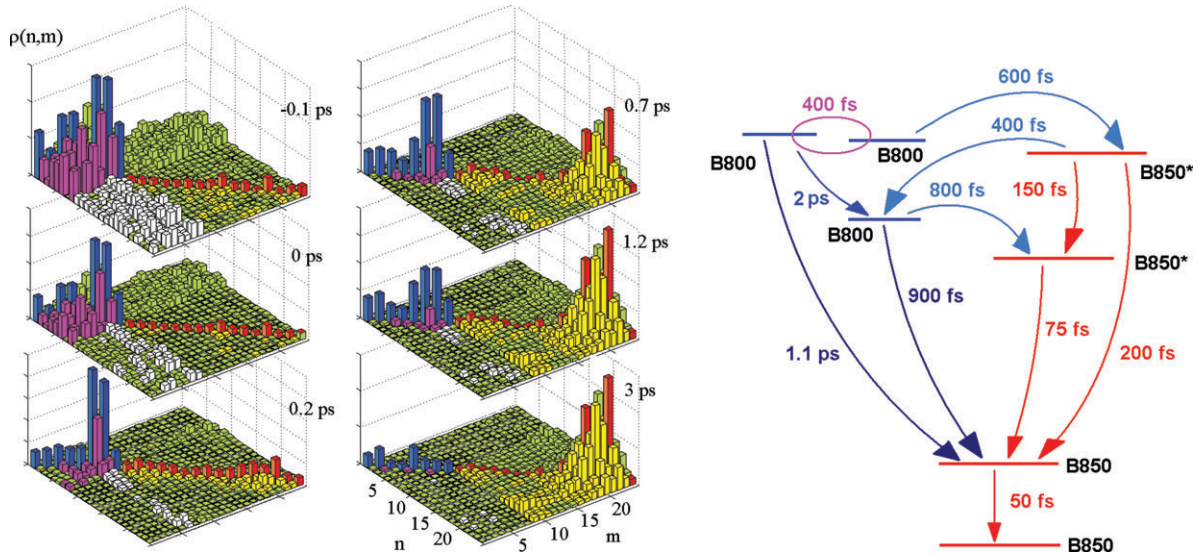

Fig. 6 Left: Dynamics of the one-exciton density matrix in the site representation upon blue-side excitation (788 nm) of the B800 band for one particular realization of the disorder. The absolute values of the density matrix elements $\rho(n,m)$ are shown for the time delays of 0.1, 0, 0.2, 0.7, 1.2, and 3 ps. We number the sites as n = 1–8 for BChl's 800 and n = 9–24 for BChl's 850 molecules (n = 1, m = 1 corresponds to the left-top corner of the panels). The BChl's 800 population and coherences are shown by blue and pink, respectively; BChl's 850 population and coherences—by red and yellow, and BChl's 800–850 coherences—by white. Right: The exciton energy level scheme and the averaged (over disorder and over levels within the corresponding subbands) relaxation time constants for 77 K. For simplicity each of the B800, B850* and B850 manifolds is represented by two levels corresponding to the blue and red side of the band. At the blue side of the B800 band two coherently excited levels are indicated.

some population of the BChl's 850 due to direct excitation of the B850* states and some coherence between BChl's 800 and 850 due to coherent superposition of the B800 and B850* states. Subsequently, the polarization approaches a stationary limit, and the pulse starts to feel the overlap between its spectrum and the absorption spectrum. From this point on (from 0 ps delay) only those site populations grow in amplitude that are in resonance with the pump. In the example shown the initial population is delocalized over the n = 6–7 dimer (with pronounced populations $\rho(6,6)$, $\rho(7,7)$ and coherences $\rho(6,7)$, $\rho(7,6)$ as shown in the 0.2 ps panel).

From 0.2 to 1.2 ps, when the antenna is no longer interacting with the pump, the coherences between BChl's 800 decay rapidly, leading to the formation of an almost localized (diagonal) density matrix in the n,m = 1–8 region. This coherence decay is accompanied by a decrease of the anisotropy with the same time constant (see fast anisotropy decay between 0 and 1 ps in Fig. 5). It is important to note that there is no significant migration around the outer BChl800 ring during this period in contrast to that suggested in earlier studies. Such a migration occurs during the period from 1.2 to 3 ps, which is characterized by significant changes in the population distribution between the n = 1–8 sites. This slow (ps) migration around the BChl800 ring from the n = 6 and 7 to n = 2 and 5 sites induces a further ps decay of anisotropy (Fig. 5).

Between 0.7 and 3 ps excitation transfer from the outer to inner ring occurs that reduces the total population of the B800 states and increases the B850 population. The final B850 wavepacket is delocalized over 5 BChl's 850.

We conclude that the quantitative model based on a simultaneous fit of linear spectra and polarized TA kinetics lead us to a more detailed picture of energy transfer in LH2 as compared with earlier models based on simplified approaches. Using the Redfield theory we adjusted the timescales of energy transfer, for example B800 → B800 transfer was found to be one order of magnitude slower than in the previous schemes. On the other hand, there exists many new relaxation channels (listed above), which were not considered by earlier models. Moreover, the modeling revealed that some kinetics components may have a completely different physical origin as compared with their original assignment. Thus, we demonstrate that the fast sub-ps component of the anisotropy decay does not reflect any population migration at all, but is connected with the coherence dynamics.

6. How energy flows in the major light-harvesting complex II of higher plants: connecting spectroscopy with the 2.72 Å crystal structure

During the last decade, following the discovery in 1994 of the crystal structure of the major antenna complex LHCII,[10] the study of the energy-transfer dynamics in the peripheral light-harvesting complexes from higher plants has attracted much attention.[157] In 1994, the LHCII structure was modeled with 3.4 Å resolution, which was not sufficient to distinguish between chlorophyll (Chl) *a* and *b* or between the X- and Y-axes of the Chls. Thus, the identities of the Chls at the twelve discernible binding sites and the directions of their dipole moments could only be assigned in a hypothetical fashion. Several site-directed mutagenesis studies of the chlorophyll binding residues allowed to determine the Chl identities.[157–161] Furthermore it was proposed that in LHCII 'mixed' sites exist, which are promiscuous in their affinity for Chls *a* and Chls *b*, although this phenomenon is a matter of controversial debate.[162]

Energy transfer from carotenoids and Chl *b* to Chl *a* in LHCII was found to be very efficient.[157] Studies of the energy transfer dynamics in LHCII by transient absorption, time-resolved fluorescence and photon echo spectroscopies revealed major components of the Chl *b* → Chl *a* transfer of 150–300 and 600 fs[46,69,163–171] together with a minor ps component. Experiments with selective excitation in the region between the absorption peaks of Chl *b* (650 nm) and Chl *a* (675 nm) provided evidence for long-lived (10–20 ps) excited states in this region.[46,164–166] The steady-state spectra were modeled with exciton theory[35,46,172,173] and possible pathways and timescales for the energy transfer were estimated using the Redfield relaxation theory.[35,46]

Recently the structure of the LHCII complex has been obtained at 2.72 Å[11] and later at 2.5 Å resolution.[12] The 14 chlorophylls (Chl) present in each monomeric subunit of LHCII were unambiguously assigned to 8 Chls *a* and 6 Chls *b* and no indication for mixed binding sites was found. Also the orientations of the Chl molecules were determined. The spectral density of coupling to low-frequency phonons can be extracted from the FLN experiment[18] as well as the frequencies and relative Huang–Rhys factors for high-frequency vibrations. (The absolute values of Huang–Rhys factors for vibrations cannot be obtained exactly[17,18] and should be scaled from the fit of a non-selective FL[46,174]). Knowledge of the effective dipole moments for Chl *a* and *b*[98] together with the spectral density of the exciton-phonon coupling[18,46] allows a quantitative calculation of the spectral and dynamic properties of the complex using one unified physical picture. Only the site energies for Chls still remain unspecified and therefore should be determined from the spectroscopic data. In a recent study[47] we presented the exciton model (with specific site energies for the 14 Chls), which allows a simultaneous and quantitative fit of all the available spectroscopic data using the modified Redfield approach.

6.1. The origin of the steady-state and transient absorption spectra

The arrangement of the Chls within the LHCII trimer according to the new crystal structure[11] is shown in Fig. 7. On the stromal side there are two tightly packed clusters of Chls *a* (red-encircled for one monomeric subunit), *i.e.* the trimer *a*610-*a*611-*a*612 and the dimer *a*602-*a*603. They are closely connected with three Chls *b* on the stromal side, Chls *b*601, *b*608, and *b*609. The structure suggests significant coupling between *b*601 and *b*609 from adjacent monomeric subunits. So, one can consider the *b*601-*b*608-*b*609 group (encircled in blue in Fig. 7) as a *b*-cluster, which is expected to have a short excited-state lifetime due to excitation energy transfer to the *a*610-*a*611-*a*612 and *a*602-*a*603 clusters of the two subunits. In the Chl *a*-region one can expect fast exciton relaxation within the *a*610-*a*611-*a*612 and *a*602-*a*603 clusters as well as slower hopping between these clusters.

On the lumenal side there are two groups of pigments *i.e.* the *a*613-*a*614 dimer (encircled by red) and the *b*605-*b*606-*b*607-

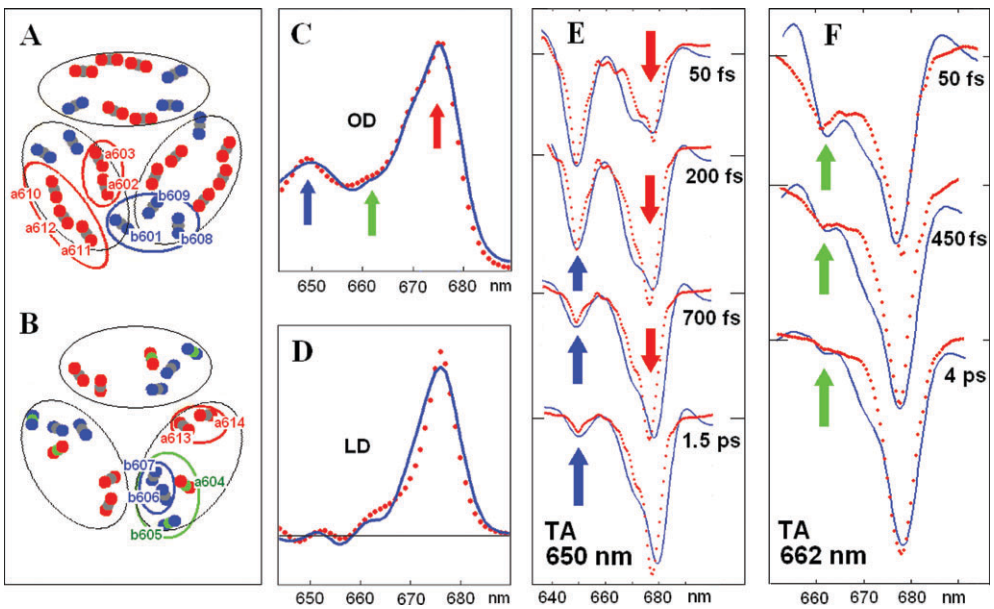

Fig. 7 Arrangement of chlorophylls within the LHC-II trimer at the stromal (A) and lumenal (B) sides. Chlorophylls are represented by three atoms: the central magnesium atom and two nitrogen atoms. The connecting line between the two nitrogens defines the directions of the Q_y transition dipole. Red, Chl *a* nitrogen; blue, Chl *b* nitrogen; grey (or green), magnesium. (according to the structure reported by Liu *et al.*[11]). Clusters of Chl's *a*, Chl's *b*, and a mixed group containing long-lived intermediate sites are encircled by red, blue, and green, respectively. The magnesium atoms for the pigments with their transition energies shifted to the intermediate region (as revealed by our modeling) are shown in green. Experimental OD and LD spectra[175] (C and D) and time-dependent TA spectra[47] (E and F) measured for the LHCII trimer at 77 K (points) and calculated with the modified Redfield theory (solid lines). E: evolution of the TA spectra upon excitation of Chl's *b* (excitation wavelength 650 nm, pulse duration 90 fs, pump–probe delays 50, 200, 700, and 1500 fs). F: dynamics of the TA upon selective excitation of the intermediate region (662 nm, 180 fs pulses, and 50, 450, and 4000 fs delays). Site energies within a monomeric subunit (E_1–E_{14}) have been adjusted in order to obtain the best simultaneous fit of the data.

*a*604 tetramer (within the green circle). The *b*605, *b*606, *b*607, and *a*604 sites of the tetramer are weakly connected to the remaining part of the complex. The excited-state dynamics within this cluster must be dominated by fast downhill transfer of excitations from the *b*-sites to the monomeric *a*604 pigment, which is the best candidate for a long-lived 'bottleneck' state, the presence of which was suggested in previous experimental studies.[164–166]

A simultaneous fit of OD, LD and TA upon different excitation wavelengths is shown in Fig. 7. The two main absorption peaks at 650 and 675 nm (shown by blue and red arrows) are determined by the Chls *b* and *a*, respectively. Excitation of the Chl *b*-band at 650 nm is followed by its sub-ps decay mirrored by the Chl *a*–band formation. The shoulder of the Chl *a* absorption near 662 nm, giving rise to a long-lived kinetic component upon 662 nm-excitation (green arrow), suggests the presence of 'bottleneck' sites, *i.e.* Chls *a* or *b* shifted to the 657–667 nm region. According to the new structure, the only sites capable of producing such a bottleneck are located within the *b*605-*b*606-*b*607-*a*604 cluster. Due to this fortunate circumstance the whole set of site energies can be better determined from the fit of the data. Knowledge of these site energies together with the experimental exciton–phonon spectral density makes it possible to determine the pathways and timescales of energy transfer in the system.

6.2. Timescales and pathways of energy transfer

The energy level diagram with the relaxation time constants for a monomeric LHCII subunit is shown in Fig. 8.

The Chl *a* region is determined by the exciton states of the *a*-clusters: three levels of the *a*610-*a*611-*a*612 trimer and two pairs of levels for the dimers *a*602-*a*603 and *a*613-*a*614 (shown in red). The wavefunctions are non-uniformly delocalized within these clusters due to the asymmetry of the unperturbed transition energies and also due to additional disorder-induced shifts of the energies. But the wavefunction overlap is still large enough to produce fast (90–300 fs) intra-cluster relaxation (shown by the red arrows). The coupling between clusters produces smaller, but sizable overlap (see for example, participation of *a*613 and *a*614 sites in the highest level of the *a*610-*a*611-*a*612 trimer, *etc.*). This gives rise to a sub-ps (250–600 fs) inter-cluster transfers in the *a*-region (shown by the brown arrows).

The Chl *b* region is characterized by a fast relaxation within the stromal-side *b*601-*b*608-*b*609 cluster (100 fs) and sub-ps transfer from this cluster to the *a*-clusters at the stromal-side, *i.e.* to the *a*610-*a*611-*a*612 trimer and *a*602-*a*603 dimer.

At the lumenal side we observe sub-ps equilibration within the *b*606-*b*607-*b*605-*a*604 group resulting in the population of the *b*605 and *a*604 pigments. The *b*605 site is then slowly depopulated *via* ps transfer to *a*604 or to the *b*601-*b*608-*b*609 cluster at the stromal side. Thus, the *b*605 is a 'bottleneck' site in the $b \rightarrow a$ energy transfer. The corresponding component in the excited state decay of a few ps can be directly observed upon selective excitation of the 655–660 nm region, as shown in Fig. 7. Another, even longer-lived 'bottleneck' site is *a*604. This site is characterized by a very slow flow of energy to the remaining *a*-sites with time-constants of 40–50 ps. An overall 12 ps-decay of the *a*604 site can be observed in the time-resolved TA-spectrum upon selective excitation of the 665–670 nm region (Palacios *et al.*, unpublished results).

Superposition of many pathways with different timescales results in the overall kinetics of the site populations shown in Fig. 8, right frame. After impulsive 650 nm excitation the three *b*-sites on the stromal side (*b*601, *b*608, and *b*609) are completely depopulated within 1 ps due to transfer to the Chl *a*-pigments. Slower components in the Chl *a*-population growth are determined by hopping between Chl *a* clusters and very slow transfer from 'bottleneck states' (populated within 0.5–1 ps from the *b*606 and *b*607 sites). In equilibrium a predominant population of the *a*610-*a*611-*a*612 cluster (mostly *a*610) is

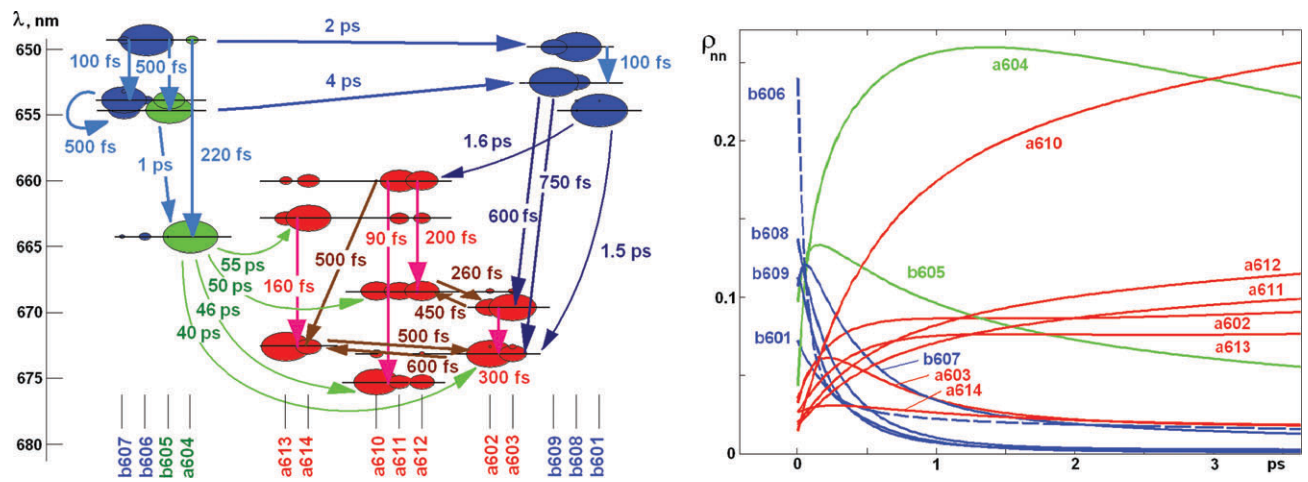

Fig. 8 Left: Energy-level diagram for a single monomeric LHCII complex. The positions (wavelengths) of the 14 exciton levels, participation of the pigments in these exciton states, and relaxation time constants are shown for one typical realization of the disorder. Parameters of the unperturbed site energies are the same as in the fit of the spectra in Fig. 7. Participation of certain pigments in each of the exciton states is shown by ellipses with the area proportional to the square of the wavefunction amplitude. Right: Dynamics of the site populations (averaged over disorder) at 77 K upon 650 nm excitation. Three groups of kinetics show populations of the *b*-sites with fast decay (blue), *a*-sites which contribute to the main absorption peak near 675 nm (red), and long-lived 'bottleneck' sites (green), *i.e.* blue-shifted Chl *a* (*a*604) and red-shifted Chl *b* (*b*605).

reached. The location of this cluster on the outer side of the LHCII trimer is likely to provide a good connection with the other subunits of PSII. Thus the current modeling with state-of-the-art physical theory provides a good description of the steady-state and time-resolved spectroscopy of the LHCII complex.

6.3. Non-photochemical quenching of excitations

Our modelling of the LHCII spectroscopy and energy transfer dynamics based on the crystal structure in principle may lead to a fundamental understanding of the process of non-photochemical quenching (NPQ), an important physiological regulation mechanism in plants that allows them to minimize the deleterious effects of exposure to excess energy.[176–179] A variety of mechanisms have been proposed, the most popular of which are: (1) quenching of the chlorophyll excited state *via* energy transfer to the S_1 level of zeaxanthin, that in excess light replaces the violoxanthin observed in the crystal structure. Since zeaxanthin has a more extended conjugated system, the S_1 energy of zeaxanthin is hypothesized to be below that of the Q_y state of the chlorophylls and thus it may act as a quencher,[176] (2) Increased aggregation of chlorophylls, either within a monomeric unit or at the interface between different monomers, leading through quenching *via* the formation of charge transfer states,[177,178] (3) charge separation between an excited chlorophyll and zeaxanthin followed by fast recombination.[179] Based on our current understanding of the energy transfer pathways in LHCII it should at least be possible to make explicit statements about the likelihood of some of these proposals. In mechanism (1) chlorophyll *a*614 is suggested to play a prominent role since it is supposed to be close to the zeaxanthin. However, in the model we propose Chl *a*614 is the main contributor to the upper-exciton state of the *a*613-*a*614 dimer and its population after 100–200 fs is relatively low, therefore. For that reason a loss channel through that site is less likely than other possibilities. In mechanism (2) the Chl *a* trimer *a*610-*a*611-*a*612 would be the site of action. The excitonic coupling between *a*612 and *a*611 is the strongest in the complex, moreover, a small change in the configuration of this dimer might mix a charge transfer state with the excited states of this trimer giving rise to a fast quenching on a timescale of tens of picoseconds. If this mechanism operates its spectroscopic signature must be observed in a more complex dynamics in the red edge of the transient absorption spectrum. Notice that charge-transfer states were not found upon LHCII aggregation,[180] implying that the quenching regime corresponds to some conformational changes within a monomeric LHCII (most probably, within tightly packed *a*610-*a*611-*a*612 cluster). In mechanism (3) charge separated states must be observed, characterized by the carotenoid cation and the chlorophyll anion. Formation of a carotenoid cation was in fact observed in leaves under conditions of NPQ.[179] The evolution of the excited state in LHCII under quenched conditions into this charge-separated state will inform us precisely about the underlying mechanism. Again, like in model (1), the involvement of *a*614 seems less likely, possibly charge separation occurs between one of the chlorophylls of the *a*610-*a*611-*a*612 trimer but then it would involve a lutein.

7. Summary and outlook

We have shown that nonlinear spectroscopy in combination with modelling based on high-resolution structure have unveiled energy transfer pathways in the bacterial antenna complexes LH1/LH2 and in the major plant light-harvesting complex LHCII. In these complexes strongly coupled clusters of light-harvesting pigments (BChl850's, Chls *a*/*b*) are present together with weakly coupled aggregates (BChl800's) or monomeric sites (Chls *a*/*b*), giving rise to complicated interplay of interband conversion and intraband dynamics including fast exciton relaxation and slow migration. Obviously, the traditional Förster theory for excitation energy transfer among weakly coupled chromophores does not work in this case. We demonstrate that a self-consistent description of the dynamics and the spectroscopy can only be obtained using a unified physical model valid for an arbitrary degree of delocalization, such as the Redfield relaxation theory. On the other hand, the energy transfers in these complexes occur between pairs of eigenstates (both localized and delocalized) in some cases separated by a small, in other cases by a large energy gap. A quantitative description of both types of energy transfer is only possible using a realistic exciton–phonon spectral density and by including, multi-phonon processes. The problem can be resolved with the modified Redfield approach, where arbitrary delocalization and arbitrary strong coupling to phonons (at least for diagonal exciton–phonon coupling) are included explicitly.

Combination of increasingly realistic physics with new experimental results provides a unique possibility to reveal the exact nature of elementary events and their interplay in a whole excitation dynamics using a global systematic modelling. We show examples of simultaneous quantitative fit of the steady-state spectra and nonlinear kinetics for the complexes under study. To make the analysis more critical to the parameter choice it is important to use a simultaneous fit of the data obtained by several complementary nonlinear spectroscopy techniques reflecting different aspects of the dynamic behaviour of the system (time- and frequency-domain techniques, pump–probe and photon echo, measurements of isotropic kinetics and anisotropy decays, *etc*.). For these complex systems such an approach reveals limitations (or even complete failure) of qualitative pictures based on fragmentary fittings.

Typically the model based on the limited data set is not unique. For example, the fit of the linear spectra of LHCII (see Fig. 7) allows finding up to three dozen models with different site energies that reproduce quantitatively all the features of the OD and LD shapes. Although most of these models fail to explain the spectral shapes and timescales of the TA kinetics, some of them still survive if we restrict the fit to the 650 nm-excitation case (reflecting interband Chl $b \rightarrow a$ conversion). Only after including into the fit the 662 nm-excitation kinetics (reflecting a slow intraband Chls *a* equilibration) can we unambiguously specify the site energies.

Besides establishing the unperturbed site energies, it is important to know the statistics of their random shifts induced by slow conformations. These shifts can have a dramatic effect on the excitation dynamics. To give an insight into the origins

of the energetic disorder it is useful to combine the bulk (ensemble-averaged) spectroscopies with the single-molecule studies.

The parameters of the antenna determined by the modeling allow determination of the pathways and timescales of energy transfer making possible a visualization of the excitation dynamics, thus leading to a consistent physical picture of how photosynthetic pigment–proteins perform their function in storing solar energy.

Acknowledgements

This research was supported by the by the Netherlands Organisation for Scientific Research (NWO) (Dutch-Russian scientific cooperation program, grant 047.016.006).

References

1 R. van Grondelle, J. P. Dekker, T. Gillbro and V. Sundström, *Biochim. Biophys. Acta*, 1994, **1187**, 1.
2 H. van Amerongen, L. Valkunas and R. van Grondelle, *Photosynthetic Excitons*, World Scientific Publishers, 2000.
3 R. E. Fenna and B. W. Matthews, *Nature*, 1975, **258**, 573.
4 G. McDermott, S. M. Prince, A. A. Freer, A. M. Hawthornthwaite-Lawless, M. Z. Papiz, R. J. Cogdell and N. W. Isaacs, *Nature*, 1995, **374**, 517.
5 J. Koepke, X. Hu, C. Muenke, K. Schulten and H. Michel, *Structure*, 1996, **4**, 581.
6 M. Z. Papiz, S. M. Prince, T. Howard, R. J. Cogdell and N. W. Isaacs, *J. Mol. Biol.*, 2003, **326**, 1523.
7 S. Karrasch, P. A. Bullough and R. Ghosh, *EMBO J.*, 1995, **14**, 631.
8 S. Scheuring, J. Seguin, S. Marco, D. Levy, B. Robert and J. L. Rigaud, *Proc. Natl. Acad. Sci. U. S. A.*, 2003, **100**, 1690.
9 A. W. Roszak, T. D. Howard, J. Southall, A. T. Gardiner, C. J. Law, N. W. Isaacs and R. J. Cogdell, *Science*, 2003, **302**, 1969.
10 W. Kühlbrandt, D. N. Wang and Y. Fujiyoshi, *Nature*, 1994, **367**, 614.
11 Z. Liu, H. Yan, K. Wang, T. Kuang, J. Zhang, L. Gui, X. An and W. Chang, *Nature*, 2004, **428**, 287.
12 J. Standfuss, M. Lamborghini, W. Kühlbrandt and A. C. T. van Scheltinga1, *EMBO J.*, 2005, **24**, 919.
13 P. Jordan, P. Fromme, H. T. Witt, O. Klukas, W. Saenger and N. Krauss, *Nature*, 2001, **411**, 909.
14 A. Zouni, H. T. Witt, J. Kern, P. Fromme, N. Krau, W. Saenger and P. Orth, *Nature*, 2001, **409**, 739.
15 N. Kamiya and J.-R. Shen, *Proc. Natl. Acad. Sci. U. S. A.*, 2003, **100**, 98.
16 K. N. Ferreira, T. M. Iverson, K. Maghlaoui, J. Barber and S. Iwata, *Science*, 2004, **303**, 1831.
17 J. Pieper, J. Voigt and G. J. Small, *J. Phys. Chem. B*, 1999, **103**, 2319.
18 E. J. G. Peterman, T. Pullerits, R. van Grondelle and H. van Amerongen, *J. Phys. Chem. B*, 1997, **101**, 4448.
19 E. J. G. Peterman, H. van Amerongen, R. van Grondelle and J. P. Dekker, *Proc. Natl. Acad. Sci. U. S. A.*, 1998, **95**, 6128.
20 J. Pieper, R. Scho1del, K.-D. Irrgang, J. Voigt and G. Renger, *J. Phys. Chem. B*, 2001, **105**, 7115.
21 M. Rätsep and A. Freiberg, *Chem. Phys. Lett.*, 2003, **377**, 371.
22 J. Pieper, K.-D. Irrgang, G. Renger and R. E. Lechner, *J. Phys. Chem. B*, 2004, **108**, 10556.
23 A. Damjanović, I. Kosztin, U. Kleinekathöfer and K. Schulten, *Phys. Rev. E*, 2002, **65**, 031919.
24 G. R. Fleming and R. van Grondelle, *Curr. Opin. Struct. Biol.*, 1997, **7**, 738.
25 V. Sundström, T. Pullerits and R. van Grondelle, *J. Phys. Chem. B*, 1999, **103**, 2327.
26 R. van Grondelle and V. Novoderezhkin, *Biochemistry*, 2001, **40**, 15057.
27 Th. Renger, V. May and O. Kühn, *Phys. Rep.*, 2001, **343**, 137.
28 X. Hu, T. Ritz, A. Damjanović, F. Autenrieth and K. Schulten, *Q. Rev. Biophys.*, 2002, **35**, 1.
29 A. G. Redfield, *Adv. Magn. Reson.*, 1965, **1**, 1.
30 O. Kühn and V. Sundström, *J. Chem. Phys.*, 1997, **107**, 4154.
31 O. Kühn, V. Sundström and T. Pullerits, *Chem. Phys.*, 2002, **275**, 15.
32 B. Brüggemann and V. May, *J. Chem. Phys.*, 2004, **120**, 2325.
33 O. Kühn and V. Sundström, *J. Phys. Chem. B*, 1997, **101**, 3432.
34 V. Novoderezhkin, M. Wendling and R. van Grondelle, *J. Phys. Chem. B*, 2003, **107**, 11534.
35 V. Novoderezhkin, J. M. Salverda, H. van Amerongen and R. van Grondelle, *J. Phys. Chem. B*, 2003, **107**, 1893.
36 Th. Renger and V. May, *J. Phys. Chem. A*, 1998, **102**, 4381.
37 S. I. E. Vulto, M. A. de Baat, S. Neerken, F. R. Nowak, H. van Amerongen, J. Amesz and T. J. Aartsma, *J. Phys. Chem. B*, 1999, **103**, 8153.
38 B. Brüggemann, K. Sznee, V. Novoderezhkin, R. van Grondelle and V. May, *J. Phys. Chem. B*, 2004, **108**, 13536.
39 J. A. Leegwater, J. R. Durrant and D. R. Klug, *J. Phys. Chem. B*, 1997, **101**, 7205.
40 V. I. Prokhorenko and A. R. Holzwarth, *J. Phys. Chem. B*, 2000, **104**, 11563.
41 L. M. C. Barter, J. R. Durrant and D. R. Klug, *Proc. Natl. Acad. Sci. U. S. A.*, 2003, **100**, 946.
42 W. M. Zhang, T. Meier, V. Chernyak and S. Mukamel, *J. Chem. Phys.*, 1998, **108**, 7763.
43 W. M. Zhang, T. Meier, V. Chernyak and S. Mukamel, *Philos. Trans. R. Soc. London, Ser. A*, 1998, **356**, 405.
44 M. Yang and G. R. Fleming, *Chem. Phys.*, 2002, **275**, 355.
45 M. Yang, A. Damjanović, H. M. Vaswani and G. R. Fleming, *Biophys. J.*, 2003, **85**, 140.
46 V. Novoderezhkin, M. Palacios, H. van Amerongen and R. van Grondelle, *J. Phys. Chem. B*, 2004, **108**, 10363.
47 V. Novoderezhkin, M. Palacios, H. van Amerongen and R. van Grondelle, *J. Phys. Chem. B*, 2005, **109**, 10493.
48 G. Raszewski, W. Saenger and T. Renger, *Biophys. J.*, 2005, **88**, 986.
49 V. I. Novoderezhkin, E. G. Andrizhiyevskaya, J. P. Dekker and R. van Grondelle, *Biophys. J.*, 2005, **89**, 1464.
50 M. Cho, H. M. Vaswani, T. Brixner, J. Stenger and G. R. Fleming, *J. Phys. Chem. B*, 2005, **109**, 10542.
51 M. H. Vos, F. Rappaport, J.-Ch. Lambry, J. Breton and J.-L. Martin, *Nature*, 1993, **363**, 320.
52 M. H. Vos, M. R. Jones, C. N. Hunter, J. Breton, J.-Ch. Lambry and J.-L. Martin, *Biochemistry*, 1994, **33**, 6750.
53 M. H. Vos, M. R. Jones, C. N. Hunter, J. Breton and J.-L. Martin, *Proc. Natl. Acad. Sci. U. S. A.*, 1994, **91**, 12701.
54 M. H. Vos, J. Breton and J.-L. Martin, *J. Phys. Chem. B*, 1997, **101**, 9820.
55 M. H. Vos, M. R. Jones and J.-L. Martin, *Chem. Phys.*, 1998, **233**, 179.
56 A. M. Streltsov, A. G. Yakovlev, A. Ya. Shkuropatov and V. A. Shuvalov, *FEBS Lett.*, 1996, **383**, 129.
57 A. M. Streltsov, S. I. E. Vulto, A. Ya. Shkuropatov, A. J. Hoff, T. J. Aartsma and V. A. Shuvalov, *J. Phys. Chem. B*, 1998, **102**, 7293.
58 D. C. Arnett, C. C. Moser, P. L. Dutton and N. F. Scherer, *J. Phys. Chem. B*, 1999, **103**, 2014.
59 M. Chachisvilis, T. Pullerits, M. R. Jones, C. N. Hunter and V. Sundström, *Chem. Phys. Lett.*, 1994, **224**, 345.
60 M. Chachisvilis, H. Fidder, T. Pullerits and V. Sundström, *J. Raman Spectrosc.*, 1995, **26**, 513.
61 M. Chachisvilis and V. Sundström, *Chem. Phys. Lett.*, 1996, **261**, 165.
62 S. E. Bradforth, R. Jimenez, F. van Mourik, R. van Grondelle and G. R. Fleming, *J. Phys. Chem.*, 1995, **99**, 16179.
63 T. Joo, Y. Jia, J.-Y. Yu, D. M. Jonas and G. R. Fleming, *J. Phys. Chem.*, 1996, **100**, 2399.
64 R. Jimenez, F. van Mourik, J.-Y. Yu and G. R. Fleming, *J. Phys. Chem. B*, 1997, **101**, 7350.
65 R. Kumble, S. Palese, R. W. Visschers, P. L. Dutton and R. M. Hochstrasser, *Chem. Phys. Lett.*, 1996, **261**, 396.
66 R. Monshouwer, A. Baltushka, F. van Mourik and R. van Grondelle, *J. Phys. Chem. A*, 1998, **102**, 4360.

67 S. Savikhin, Y. Zhu, S. Lin, R. E. Blankenship and W. S. Struve, *J. Phys. Chem.*, 1994, **98**, 10322.
68 S. Savikhin, P. I. Van Noort, Y. Zhu, S. Lin, R. E. Blankenship and W. S. Struve, *Chem. Phys.*, 1995, **194**, 245.
69 R. Agarval, B. P. Krueger, G. D. Scholes, M. Yang, J. Yom, L. Mets and G. R. Fleming, *J. Phys. Chem. B*, 2000, **104**, 2908.
70 J. M. Jean, R. A. Friesner and G. R. Fleming, *J. Chem. Phys.*, 1992, **96**, 5827.
71 J. M. Jean, *J. Chem. Phys.*, 1994, **101**, 10464.
72 J. M. Jean and G. R. Fleming, *J. Chem. Phys.*, 1995, **103**, 2092.
73 V. I. Novoderezhkin, A. G. Yakovlev, R. van Grondelle and V. A. Shuvalov, *J. Phys. Chem. B*, 2004, **108**, 7445.
74 Th. Renger and V. May, *J. Phys. Chem. B*, 1997, **101**, 7232.
75 Th. Renger and V. May, *Photochem. Photobiol.*, 1997, **66**(5), 618.
76 M. Chachisvilis and V. Sundström, *Chem. Phys. Lett.*, 1996, **261**, 165.
77 V. Novoderezhkin, R. Monshouwer and R. van Grondelle, *J. Phys. Chem. B*, 2000, **104**, 12056.
78 V. Novoderezhkin, R. Monshouwer and R. van Grondelle, *J. Phys. Chem. B*, 2002, **106**, 6025.
79 H.-M. Wu and G. Small, *Chem. Phys.*, 1997, **218**, 225.
80 H.-M. Wu and G. Small, *J. Phys. Chem. B*, 1998, **102**, 888.
81 H.-M. Wu, M. Rätsep, R. Jankowiak, R. J. Cogdell and G. J. Small, *J. Phys. Chem. B*, 1997, **101**, 7641.
82 Y. Jung, E. Barkai and R. J. Silbey, *J. Chem. Phys.*, 2002, **117**, 10980.
83 E. Barkai, Y. J. Jung and R. J. Silbey, *Annu. Rev. Phys. Chem.*, 2004, **55**, 457.
84 M. A. Bopp, Y. Jia, L. Li, R. J. Cogdell and R. M. Hochstrasser, *Proc. Natl. Acad. Sci. U. S. A.*, 1997, **94**, 10630.
85 M. A. Bopp, A. Sytnik, T. D. Howard, R. J. Cogdell and R. M. Hochstrasser, *Proc. Natl. Acad. Sci. U. S. A.*, 1999, **96**, 11271.
86 A. M. van Oijen, M. Ketelaars, J. Köhler, T. J. Aartsma and J. Schmidt, *Phys. Chem. B*, 1998, **102**, 9363.
87 A. M. van Oijen, M. Ketelaars, J. Köhler, T. J. Aartsma and J. Schmidt, *Science*, 1999, **285**, 400.
88 A. M. van Oijen, M. Ketelaars, J. Köhler, T. J. Aartsma and J. Schmidt, *Chem. Phys.*, 1999, **247**, 53.
89 C. Tietz, O. Chekhlov, A. Dräbenstedt, J. Schuster and J. Wrachtrup, *J. Phys. Chem. B*, 1999, **103**, 6328.
90 M. Ketelaars, A. M. van Oijen, M. Matsushita, J. Köhler, J. Schmidt and T. J. Aartsma, *Biophys. J.*, 2001, **80**, 1591.
91 U. Gerken, F. Jelezko, B. Götze, M. Branschädel, C. Tietz, R. Ghosh and J. Wrachtrup, *J. Phys. Chem. B*, 2003, **107**, 338.
92 U. Gerken, D. Lupo, C. Tietz, J. Wrachtrup and R. Ghosh, *Biochemistry*, 2003, **42**, 10354.
93 C. Hofmann, F. Francia, G. Venturoli, D. Oesterhelt and J. Köhler, *FEBS Lett.*, 2003, **546**, 345.
94 D. Rutkauskas, V. Novoderezhkin, R. J. Cogdell and R. van Grondelle, *Biochemistry*, 2004, **43**, 4431.
95 D. Rutkauskas, V. Novoderezhkin, R. J. Cogdell and R. van Grondelle, *Biophys. J.*, 2005, **88**, 422.
96 M. V. Mostovoy and J. Knoester, *J. Phys. Chem. B*, 2000, **104**, 12355.
97 M. Matsushita, M. Ketelaars, A. M. van Oijen, J. Köhler, T. J. Aartsma and J. Schmidt, *Biophys. J.*, 2001, **80**, 1604.
98 R. S. Knox and B. Q. Spring, *Photochem. Photobiol.*, 2003, **77**, 497.
99 M. Wendling, F. van Mourik, I. H. M. van Stokkum, J. M. Salverda, H. Michel and R. van Grondelle, *Biophys. J.*, 2003, **84**, 440.
100 R. Monshouwer, M. Abrahamsson, F. van Mourik and R. van Grondelle, *J. Phys. Chem. B*, 1997, **101**, 7241.
101 H. van der Laan, Th. Schmidt, R. W. Visschers, K. J. Visscher, R. van Grondelle and S. Völker, *Chem. Phys. Lett.*, 1990, **170**, 231.
102 N. R. S. Reddy, G. J. Small, M. Seibert and R. Picorel, *Chem. Phys. Lett.*, 1991, **181**, 391.
103 C. D. de Caro, R. W. Visschers, R. van Grondelle and S. Völker, *J. Phys. Chem.*, 1994, **98**, 10584.
104 H.-M. Wu, S. Savikhin, N. R. S. Reddy, R. Jankowiak, R. J. Cogdell and G. J. Small, *J. Phys. Chem.*, 1996, **100**, 12022.
105 S. Matsuzaki, V. Zazubovich, N. J. Fraser, N. J. R. J. Cogdell and G. J. Small, *J. Phys. Chem. B*, 2001, **105**, 7049.
106 V. Zazubovich, R. Jankowiak and G. J. Small, *J. Lumin.*, 2002, **98**, 123.
107 S. Hess, F. Feldchtein, A. Babin, I. Nurgaleev, T. Pullerits, A. Sergeev and V. Sundström, *Chem. Phys. Lett.*, 1993, **216**, 247.
108 S. Hess, E. Åkesson, R. J. Cogdell, T. Pullerits and V. Sundström, *Biophys. J.*, 1995, **69**, 2211.
109 R. Monshouwer, I. Ortiz de Zarate, F. van Mourik and R. van Grondelle, *Chem. Phys. Lett.*, 1995, **246**, 341.
110 Y. Z. Ma, R. J. Cogdell and T. Gillbro, *J. Phys. Chem. B*, 1997, **101**, 1087.
111 Y. Z. Ma, R. J. Cogdell and T. Gillbro, *J. Phys. Chem. B*, 1998, **102**, 881.
112 J. T. M. Kennis, A. M. Streltsov, T. J. Aartsma, T. Nozava and J. Amesz, *J. Phys. Chem.*, 1996, **100**, 2438.
113 J. T. M. Kennis, A. M. Streltsov, S. I. E. Vulto, T. J. Aartsma, T. Nozava and J. Amesz, *J. Phys. Chem. B*, 1997, **101**, 7827.
114 T. Pullerits, S. Hess, J. L. Herek and V. Sundström, *J. Phys. Chem. B*, 1997, **101**, 10560.
115 J. A. Ihalainen, J. Linnanto, P. Myllyperkiö, I. H. M. van Stokkum, B. Ücker, H. Scheer and J. E. I. Korppi-Tommola, *J. Phys. Chem. B*, 2001, **105**, 9849.
116 J. M. Salverda, F. van Mourik, G. van der Zwan and R. van Grondelle, *J. Phys. Chem. B*, 2000, **104**, 11395.
117 R. Agarwal, M. Yang, Q. H. Xu and G. R. Fleming, *J. Phys. Chem. B*, 2001, **105**, 1887.
118 R. W. Visschers, L. Germeroth, H. Michel, R. Monshouwer and R. Grondelle, *Biochim. Biophys. Acta*, 1995, **1230**, 147.
119 N. R. S. Reddy, R. Picorel and G. J. Small, *J. Phys. Chem.*, 1992, **96**, 6458.
120 N. R. S. Reddy, R. J. Cogdell, L. Zhao and G. J. Small, *Photochem. Photobiol.*, 1993, **57**, 35.
121 H.-M. Wu, N. R. S. Reddy and G. J. Small, *J. Phys. Chem. B*, 1997, **101**, 651.
122 M. H. C. Koolhaas, G. van der Zwan, R. N. Frese and R. van Grondelle, *J. Phys. Chem. B*, 1997, **101**, 7262.
123 M. H. C. Koolhaas, R. N. Frese, G. J. S. Fowler, T. S. Bibby, S. Georgakopoulou, G. van der Zwan, C. N. Hunter and R. van Grondelle, *Biochemistry*, 1998, **37**, 4693.
124 S. Georgakopoulou, R. N. Frese, E. Johnson, M. H. C. Koolhaas, R. J. Cogdell, R. van Grondelle and G. van der Zwan, *Biophys. J.*, 2002, **82**, 2184.
125 L. M. P. Beekman, R. N. Frese, G. J. S. Fowler, R. Picorel, R. J. Cogdell, I. H. M. van Stokkum, C. N. Hunter and R. van Grondelle, *J. Phys. Chem. B*, 1997, **101**, 7293.
126 R. Jimenez, S. N. Dikshit, S. E. Bradforth and G. R. Fleming, *J. Phys. Chem.*, 1996, **100**, 6825.
127 V. Novoderezhkin, R. Monshouwer and R. van Grondelle, *J. Phys. Chem. B*, 1999, **103**, 10540.
128 V. Nagarajan, R. G. Alden, J. C. Williams and W. W. Parson, *Proc. Natl. Acad. Sci. U. S. A.*, 1996, **93**, 13774.
129 V. Nagarajan, E. T. Johnson, J. C. Williams and W. W. Parson, *J. Phys. Chem. B*, 1999, **103**, 2297.
130 M. Chachisvilis, O. Kühn, T. Pullerits and V. Sundström, *V. J. Phys. Chem. B*, 1997, **101**, 7275.
131 S. I. E. Vulto, J. T. M. Kennis, A. M. Streltsov, J. Amesz and T. J. Aartsma, *J. Phys. Chem. B*, 1999, **103**, 878.
132 R. G. Alden, E. Johnson, V. Nagarajan, W. W. Parson, C. J. Law and R. J. Cogdell, *J. Phys. Chem. B*, 1997, **101**, 4667.
133 G. D. Scholes, I. R. Gould, R. J. Cogdell and G. R. Fleming, *J. Phys. Chem. B*, 1999, **103**, 2543.
134 S. Tretiak, C. Middleton, V. Chernyak and S. Mukamel, *J. Phys. Chem. B*, 2000, **104**, 4519.
135 S. Tretiak, C. Middleton, V. Chernyak and S. Mukamel, *J. Phys. Chem. B*, 2000, **104**, 9540.
136 V. I. Novoderezhkin and A. P. Razjivin, *FEBS Lett.*, 1993, **330**, 5.
137 V. I. Novoderezhkin and A. P. Razjivin, *Photosynth. Res.*, 1994, **42**, 9.
138 V. I. Novoderezhkin and A. P. Razjivin, *FEBS Lett.*, 1995, **368**, 370.
139 T. Pullerits, M. Chachisvilis and V. Sundström, *J. Phys. Chem.*, 1996, **100**, 10787.
140 T. V. Dracheva, V. I. Novoderezhkin and A. P. Razjivin, *Chem. Phys.*, 1995, **194**, 223.
141 T. V. Dracheva, V. I. Novoderezhkin and A. P. Razjivin, *Photochem. Photobiol.*, 1997, **66**(4), 141.
142 A. Freiberg, M. Rätsep, K. Timpmann and G. Trinkunas, *J. Lumin.*, 2003, **102–103**, 363.

143 T. Meier, V. Chernyak and S. Mukamel, *J. Phys. Chem. B*, 1997, **101**, 7332.
144 M. Dahlbom, T. Pullerits, S. Mukamel and V. Sundström, *J. Phys. Chem. B*, 2001, **105**, 5515.
145 W. Xiao, S. Lin, A. K. W. Taguchi and N. W. Woodbury, *Biochemistry*, 1994, **33**, 8313.
146 H. M. Visser, O. J. G. Somsen, F. van Mourik, S. Lin, I. H. M. van Stokkum and R. van Grondelle, *Biophys. J.*, 1995, **69**, 1083.
147 H. M. Visser, O. J. G. Somsen, F. van Mourik, S. Lin, I. H. M. van Stokkum and R. van Grondelle, *J. Phys. Chem.*, 1996, **100**, 18859.
148 S. Savikhin and W. S. Struve, *Chem. Phys.*, 1996, **210**, 91.
149 J. T. M. Kennis, A. M. Streltsov, H. Permentier, T. J. Aartsma and J. Amesz, *J. Phys. Chem. B*, 1997, **101**, 8369.
150 T. Polívka, T. Pullerits, J. L. Herek and V. Sundström, *J. Phys. Chem. B*, 2000, **104**, 1088.
151 L. D. Book, A. E. Ostafin, N. Ponomarenko, J. R. Norris and N. F. Scherer, *J. Phys. Chem. B*, 2000, **104**, 8295.
152 V. Novoderezhkin, R. Monshouwer and R. van Grondelle, *Biophys. J.*, 1999, **77**, 666.
153 H. Sumi, *J. Phys. Chem. B*, 1999, **103**, 252.
154 K. Mukai, S. Abe and H. Sumi, *J. Phys. Chem. B*, 1999, **103**, 6069.
155 G. D. Scholes and G. R. Fleming, *J. Phys. Chem. B*, 2000, **104**, 1854.
156 S. Jang, M. D. Newton and R. J. Silbey, *Phys. Rev. Lett.*, 2004, **92**, 218301.
157 H. van Amerongen and R. van Grondelle, *J. Phys. Chem. B*, 2001, **105**, 604.
158 R. Remelli, C. Varotto, D. Sandona, R. Croce and R. Bassi, *J. Biol. Chem.*, 1999, **274**, 33510.
159 H. Rogl and W. Kühlbrandt, *Biochemistry*, 1999, **38**, 16214.
160 C. Yang, K. Kosemund, C. Cornet and H. Paulsen, *Biochemistry*, 1999, **38**, 16205.
161 H. Rogl, R. Schödel, H. Lokstein, W. Kühlbrandt and A. Schubert, *Biochemistry*, 2002, **41**, 2281.
162 R. Bassi, R. Croce, D. Cugini and D. Sandona, *Proc. Natl. Acad. Sci. U. S. A.*, 1999, **96**, 10056.
163 T. Bittner, G. P. Wiederrecht, K.-D. Irrgang, G. Renger and M. R. Wasielewski, *Chem. Phys.*, 1995, **194**, 311.
164 H. M. Visser, F. J. Kleima, I. H. M. van Stokkum, R. van Grondelle and H. van Amerongen, *J. Chem. Phys.*, 1996, **210**, 297.
165 F. J. Kleima, C. C. Gradinaru, F. Calkoen, I. H. M. van Stokkum, R. van Grondelle and H. van Amerongen, *Biochemistry*, 1997, **36**, 15262.
166 C. C. Gradinaru, S. Özdemir, D. Gülen, I. H. M. van Stokkum, R. van Grondelle and H. van Amerongen, *Biophys. J.*, 1998, **75**, 3064.
167 C. C. Gradinaru, I. H. M. van Stokkum, A. A. Pascal, R. van Grondelle and H. van Amerongen, *Phys. Chem. B*, 2000, **104**, 9330.
168 M. Du, X. Xie, L. Mets and G. R. Fleming, *Phys. Chem.*, 1994, **98**, 4736.
169 T. Bittner, K.-D. Irrgang, G. Renger and M. R. Wasielewski, *J. Phys. Chem.*, 1994, **98**, 11821.
170 J. P. Connelly, M. G. Müller, M. Hucke, G. Gatzen, C. W. Mullineaux, A. V. Ruban, P. Horton and A. R. Holzwarth, *J. Phys. Chem. B*, 1997, **101**, 1902.
171 J. M. Salverda, M. Vengris, B. P. Krueger, G. D. Scholes, A. R. Czarnoleski, V. Novoderezhkin, H. van Amerongen and R. van Grondelle, *Biophys. J.*, 2003, **84**, 450.
172 Th. Renger and V. May, *Phys. Rev. Lett.*, 2000, **84**, 5228.
173 E. I. İşeri and D. Gülen, *Eur. Biophys. J.*, 2001, **30**, 344.
174 M. A. Palacios, F. L. de Weerd, J. A. Ihalainen, R. van Grondelle and H. van Amerongen, *J. Phys. Chem. B*, 2002, **106**, 5782.
175 H. van Amerongen, S. L. S. Kwa, B. M. van Bolhuis and R. van Grondelle, *Biophys. J.*, 1994, **67**, 837.
176 H. A. Frank, A. Cua, V. Chynwat, A. Young, D. Gosztola and M. R. Wasielewski, *Photosynth. Res.*, 1994, **41**, 389.
177 P. Horton, A. Ruban and R. G. Walters, *Annu. Rev. Plant Physiol.*, 1996, **47**, 655.
178 A. A. Pascal, Z. F. Liu, K. Broess, B. van Oort, H. van Amerongen, C. Wang, P. Horton, B. Robert, W. R. Chang and A. Ruban, *Nature*, 2005, **436**, 134.
179 N. E. Holt, D. Zigmantas, L. Valkunas, X.-P. Li, K. K. Niyogi and G. R. Fleming, *Science*, 2005, **307**, 433.
180 A. M. Palacios, R. N. Frese, C. C. Gradinaru, I. H. M. van Stokkum, L. L. Premvardhan, P. Horton, A. V. Ruban, R. van Grondelle and H. van Amerongen, *Biochim. Biophys. Acta*, 2003, **1605**, 83.